BAMS Article

The Use and Potential of Far-Infrared Remote Sensing in Deriving Surface Longwave Downward Radiation under Clear-Sky Conditions

Yihan Du,[a,c] Tianxing Wang,[b,d,e] Dahui Li,[b] Yi Zheng,[a] Yuyang Xian,[b] and Stefan A. Buehler[c]

KEYWORDS:
Atmosphere;
Infrared radiation;
Longwave radiation;
Radiation budgets;
Radiative transfer;
Remote sensing

ABSTRACT: Surface longwave downward radiation (LWDR) is an essential parameter in Earth's radiation balance and climate change studies. To date, almost all existing space-based LWDR studies mainly focus on the traditional thermal infrared (TIR) spectrum of 4–15 μm. The far-infrared (FIR) spectrum (>15 μm), with its high sensitivity to temperature and water vapor, has the potential to greatly improve the derivation accuracy of LWDR, which is closely related to the above variables. This study proposes a novel attempt to estimate clear-sky LWDR by integrating the traditional TIR bands and newly selected FIR bands. Through comprehensive simulations and analyses, we identify that the FIR bands can serve as an essential complement to existing TIR-based methods, thereby significantly improving the accuracy of LWDR estimation and yielding a 16% overall accuracy improvement. This substantial potential for enhanced accuracy is particularly evident under conditions of low water vapor content or in polar atmospheres, where improvements exceed 23%. This research represents the first incorporation of FIR into longwave radiation estimation fields, highlighting a promising advancement in remote sensing techniques. The findings inspire further exploration of FIR's potential and lay the groundwork for a deeper understanding of LWDR and the complexities of Earth's radiation balance, ultimately aiding in more accurate assessments of climate change.

SIGNIFICANCE STATEMENT: Integrating far-infrared into longwave downward radiation estimation marks a significant advancement beyond traditional thermal infrared methods. This study demonstrates that adding FIR data greatly enhances longwave downward radiation (LWDR) accuracy, especially in extreme environments like polar regions and areas with low water vapor, where TIR alone struggles to provide precise estimates. With improving accuracy by up to 23% in polar regions and 16% globally, this approach offers a more reliable understanding of Earth's radiation budget. These findings are crucial for refining climate models and designing future satellite missions, ultimately supporting better climate predictions and strategies to address climate change.

DOI: 10.1175/BAMS-D-24-0259.1
Corresponding author: Tianxing Wang, wangtx23@mail.sysu.edu.cn
Manuscript received 17 September 2024, in final form 3 June 2025, accepted 12 June 2025

AFFILIATIONS: [a] Guangdong Provincial Key Laboratory of Geodynamics and Geohazards, School of Earth Sciences and Engineering, Sun Yat-Sen University, Zhuhai, China; [b] School of Geospatial Engineering and Science, Sun Yat-sen University & Southern Marine Science and Engineering Guangdong Laboratory (Zhuhai), Zhuhai, China; [c] Meteorological Institute, Center for Earth System Research and Sustainability (CEN), University of Hamburg, Hamburg, Germany; [d] Key Laboratory of Comprehensive Observation of Polar Environment (Sun Yat-sen University), Ministry of Education, Zhuhai, China; [e] Key Laboratory of Natural Resources Monitoring in Tropical and Subtropical Area of South China, Ministry of Natural Resources, Guangzhou, China

1. Introduction

Earth's radiation balance is the main parameter that determines the climate (Wild et al. 2013). Surface longwave downward radiation (LWDR) (4–100 μm) is a key component of this balance, directly indicating the radiative heating imposed by the atmosphere on the surface (Liang et al. 2019).

Despite advances in remote sensing and climate modeling, LWDR remains one of the most challenging radiation components to retrieve accurately (Stephens et al. 2012; Trenberth and Fasullo 2012; Trenberth et al. 2009; Wang and Dickinson 2013; Wild et al. 2013). This is mainly due to its dependence on the vertical distribution of atmospheric components, particularly near-surface water vapor (WV) and temperature (Inamdar and Ramanathan 1997; Schmetz 1989). In cold and dry environments such as the poles and high-altitude regions, these variables are more difficult to estimate, leading to larger uncertainties (Jiao and Mu 2022; Ruckstuhl et al. 2007; Yan et al. 2011; Yang et al. 2006). However, improving LWDR estimates in such regions is especially important, as its greenhouse-driven amplification has been recognized as a key contributor to Arctic surface warming and sea ice decline (Cao et al. 2022; Kapsch et al. 2013; Lee et al. 2017). Traditionally, efforts to retrieve LWDR have focused on the thermal infrared (TIR) spectrum, particularly in the 8–14 μm atmospheric window, where transmittance is relatively high under most conditions (Miller et al. 2023; Xie et al. 2022). However, retrievals relying solely on TIR are prone to compensating biases, where errors in different estimated properties can offset each other or be masked across spectral bands. Although such retrievals may yield results that match observations, they obscure the true radiative contributions of individual components and the potential contribution of the far-infrared (FIR) (Feldman et al. 2014; Harries et al. 2008; Huang et al. 2013, 2007; Palchetti et al. 2020; Peterson et al. 2019).

Although historically less studied than the TIR, FIR (>15 μm) radiation accounts for a significant portion of Earth's thermal radiation budget, approximately half globally (Harries et al. 2008). This contribution exceeds 60% in cold and dry regions like the poles and high-altitude areas (L'Ecuyer et al. 2021), precisely the conditions where LWDR estimation proves most challenging. While the FIR spectrum is generally opaque due to strong WV absorption (Miller et al. 2023; Xie et al. 2022), low WV conditions, which are common in high-altitude and high-latitude regions (Xie et al. 2022), can give rise to partially transparent spectral regions known as "dirty windows"(Chen and Liu 2016; Feldman et al. 2014; Rathke et al. 2002). These windows exhibit higher transmittance, creating new opportunities for satellite remote sensing and making FIR observations possible under typically challenging conditions.

Early satellite observations of FIR, such as those from *Nimbus-3* and *Nimbus-4* in the 1970s, provided FIR observations up to 25 μm, which were limited by resolution and mission duration (Conrath et al. 1970; Hanel et al. 1971). However, these early missions were largely exploratory and lacked the operational lifespan and measurement accuracy required for quantitative climate change monitoring (Xie et al. 2023). Due to high costs and technological limitations, subsequent efforts in FIR remote sensing were largely restricted to broadband measurements or field experiments (Bianchini et al. 2019; L'Ecuyer et al. 2021; Mlynczak et al. 2016; Palchetti et al. 2021, 2020). Recent technological advances are changing this landscape. To bridge the gap in FIR remote sensing observations, two satellite missions are poised to initiate a new era. The Polar Radiant Energy in the FIR Experiment (PREFIRE) mission (L'Ecuyer et al. 2021), launched in 2024, provides systematic FIR measurements from 5 to 54 μm, primarily focusing on polar regions. Meanwhile, the Far-Infrared Outgoing Radiation Understanding and Monitoring (FORUM) (Palchetti et al. 2020) is scheduled for launch in late 2027. FORUM will deliver the first spectrally resolved observations in the 100–1600 cm^{-1} (equivalent to 100–6.25 μm) spectral range. These missions are expected to enhance understanding of the energy budget and the role of FIR in processes such as sea ice loss, ice sheet melting, and ocean dynamics. Recently, the sensitivity of FIR to cloud properties, WV, and surface temperature (ST)—key factors for estimating LWDR—has begun to attract attention, along with its application in retrieving these variables (Belotti et al. 2023; Bertossa et al. 2023; Cox et al. 2010; Di Natale et al. 2020; Martinazzo and Maestri 2023; Miller et al. 2023; Palchetti et al. 2020; Peterson et al. 2022; Turner et al. 2012a,b). However, the potential of FIR for improving LWDR estimation remains largely unexplored.

This study aims to improve LWDR estimation by integrating the underexplored FIR channels with the traditionally utilized TIR channels [e.g., Moderate Resolution Imaging Spectroradiometer (MODIS) bands], addressing the limitations of current TIR-based methods and tapping the great potential of FIR measurements. It will facilitate a deeper understanding of the mechanisms and processes of Earth's radiation balance, providing a scientific basis for deeply understanding climate change.

2. Data and simulation basics

a. Emissivity spectra and atmospheric profiles. Surface spectral emissivity directly determines surface radiation intensity and radiative flux. However, measurement data for FIR surface emissivity are scarce. Building on the FIR spectral studies by Chen et al. (2014) and Feldman et al. (2014), Huang et al. (2016) developed a global surface spectral emissivity dataset that covers the entire longwave spectrum for typical surface types. This dataset has been widely adopted in related studies of the PREFIRE mission (Bertossa et al. 2023; Huang et al. 2025; L'Ecuyer et al. 2021; Miller et al. 2023; Peterson et al. 2022; Xie et al. 2022). Based on the similarity of emissivity spectral curves, 16 representative surface spectral curves were extracted (Figs. 1a–c). From the Thermodynamic Initial Guess Retrieval (TIGR) (Chedin et al. 1985; Chevallier et al. 1998), 946 clear-sky entries were screened based on surface temperature and water vapor distribution. After quality screening and inspection, 89 profiles were selected (Fig. 1d). These profiles encompass five atmospheric types: tropical, midlatitude summer, midlatitude winter, polar summer, and polar winter.

b. Potential bands configuration and selection. Due to the limited availability of publicly accessible FIR remote sensing observation data, simulating new FIR bands is essential for supporting LWDR estimation. Band responses are constructed based on the method of Sobrino and Jiménez-Muñoz (2014) and Zheng et al. (2019), utilizing filter functions that

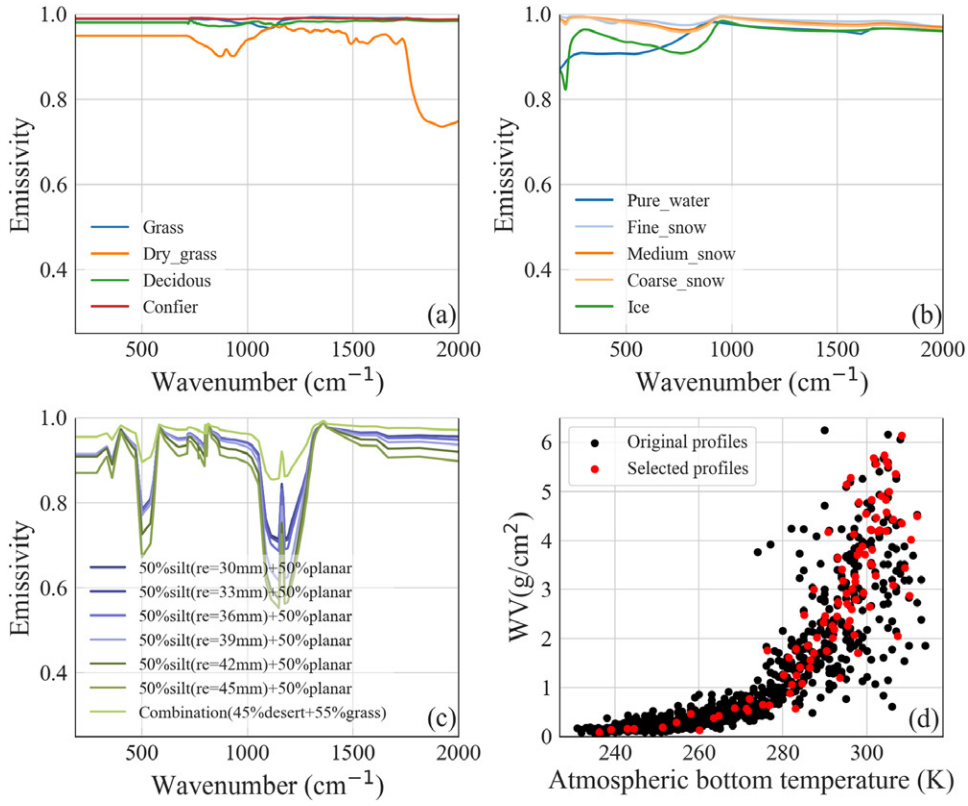

Fig. 1. (a) Spectral emissivity of vegetation. (b) Spectral emissivity of water and snow/ice. (c) Spectral emissivity of selected desert surface types. (d) The distribution of clear-sky TIGR atmospheric profiles and the chosen profiles.

are composites of Gaussian and triangular functions (Fig. 2). Considering the observation ranges of the PREFIRE and FORUM missions and publicly available channel configurations, the spectral range from 5 to 54 μm was selected, with a channel center spacing of 0.84 μm and an initial full width at half maximum (FWHM) of 0.42 μm. This configuration aligns with the planned observations of the PREFIRE mission. It is fully encompassed by the spectral coverage of the FORUM mission, which spans from 6.25 to 100 μm and provides a higher spectral resolution (~0.5 cm^{-1}). Therefore, the selected configuration facilitates forward modeling based on PREFIRE specifications and future validation using FORUM's finer spectral sampling and lower uncertainty.

MODIS has been widely used in recent years for remote sensing estimation of LWDR. To comprehensively evaluate the performance of TIR and FIR in LWDR estimation, radiation simulations were conducted for TIR using MODIS longwave bands (bands 27–36) based on the published spectral response functions (https://mcst.gsfc.nasa.gov/calibration/parameters).

The signal-to-noise ratio (SNR) quantifies the effective information content of a channel in the presence of noise and serves as the foundation for more comprehensive information content analyses (Chang et al. 2017; Rodgers 2000). This study utilized the noise equivalent temperature difference (NEΔT) specific to each MODIS band. In the main analysis, a NEΔT of 0.35 K was applied to the simulated FIR measurements. This value, consistent with the NEΔT used for MODIS bands in the

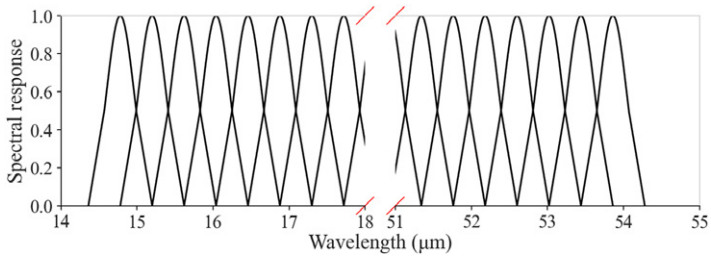

Fig. 2. Simulated channel spectral response functions; the central region (18.0–51.0 μm) is omitted for clarity.

near-far-infrared range, represents an idealized simplification for the FIR. The employed formula is as follows:

$$\mathrm{SNR} = \frac{\Delta \mathrm{BT}_{\mathrm{signal},\nu}}{\mathrm{NE}\Delta T_{\nu}}, \tag{1}$$

where $\Delta \mathrm{BT}_{\mathrm{signal},\nu}$ represents the brightness temperature (BT) change caused by variations in atmospheric conditions and ν denotes the band position or the central wavelength of the spectral band.

Information from the PREFIRE mission suggests that achieving this NEΔT across FIR channels may be challenging, particularly in polar atmospheric conditions. However, with higher spectral resolution and the potential for spectral averaging, upcoming missions such as FORUM (with 0.5 cm^{-1} resolution) may achieve lower noise levels in the FIR (Agocs et al. 2022; Miller et al. 2023). A more conservative evaluation of FIR's potential capabilities under higher noise conditions (NEΔT = 1.5 K for FIR) is presented in appendix A.

Bands with SNR values greater than the mean were retained for further analysis. Considering that the primary objective of this study is to establish a theoretical framework for exploring the potential of FIR channels in LWDR retrieval, all configurations are based on theoretical simplifications derived from currently available public information. Accordingly, a simple and stable method was adopted for band selection. Following the initial selection, a Jacobian-based sensitivity analysis was performed to estimate each band's relative contribution to LWDR retrieval. By prioritizing bands with higher sensitivity and lower redundancy through an iterative refinement strategy, the robustness and efficiency of the selection were further enhanced. Ultimately, seven MODIS bands, eight FIR bands, and nine joint bands (five MODIS and four FIR) were selected (Table 1), and their performance was further tested to ensure reliability in LWDR retrieval. Including too many bands can increase the computational complexity of the retrieval algorithm. Additionally, highly correlated bands may provide redundant information. Therefore, the selection focused on minimizing the number of bands while ensuring optimal accuracy.

c. Algorithm and validation strategy. Based on the moderate resolution atmospheric transmission (MODTRAN) 6 radiative transfer model (Berk et al. 2015), selected FIR bands and MODIS TIR bands were integrated to simulate LWDR under various atmospheric and surface conditions. For each band, the BT at the top of the atmosphere (TOA) was calculated, generating a representative dataset that captures the global distribution of LWDR. The lookup table (LUT) method was used to estimate clear-sky LWDR, ensuring methodological accuracy and adherence to atmospheric radiative transfer mechanisms (appendix B). Finally, the theoretical accuracy of clear-sky LWDR retrievals was validated using the random simulated dataset (appendix B). The accuracy of LWDR derived from several band types was evaluated using three statistical metrics: bias, root-mean-square error (RMSE), and correlation coefficient (R).

3. Comprehensive characterization of LWDR

a. Performance of LWDR derivation by incorporating FIR bands. As stated above, bands with poor SNR can deteriorate the retrieval result for the chosen LUT method because they increase complexity and inject noise without providing significant additional information. The LUT method is not good at coping with this. Indeed, the selected seven MODIS bands significantly outperform the full set of ten MODIS longwave bands in terms of retrieval accuracy, thereby corroborating the effectiveness of the band selection method (Fig. 3).

Table 1. Composition and specifications of selected MODIS and FIR bands.

	Band	Central wavelength (μm)	NEΔT (K)	MODIS (7 bands)	FIR (8 bands)	Joint (9 bands)
MODIS	27	6.770	0.25	√		
	28	7.343	0.25	√		√
	29	8.529	0.05	√		√
	30	9.735	0.25			
	31	11.012	0.05	√		√
	32	12.033	0.05	√		√
	33	13.365	0.25	√		√
	34	13.684	0.25	√		
	35	13.912	0.25			
	36	14.916	0.35			
FIR	—	17.30	0.35		√	
		17.72			√	√
		18.14			√	
		18.56			√	√
		18.99			√	
		20.25			√	√
		20.67			√	√
		21.10			√	

Consequently, only the optimized seven MODIS bands were utilized in subsequent analyses, omitting the more redundant 10-band combination.

WV is a critical factor influencing the accuracy of LWDR retrievals (Cheng et al. 2017). However, there remains considerable potential for improving LWDR retrieval accuracy under low WV conditions (Jiao and Mu 2022; Kratz et al. 2020). Under cold, dry conditions with very low WV, FIR-transparent microwindows within the 17–33 μm range introduce uncertainties in traditional clear-sky LWDR models based on TIR data (Marty et al. 2003). Under these conditions, FIR bands provide additional supplemental information through transparent microwindows, making them particularly advantageous in polar regions. As Fig. 3 shows, joint bands significantly improve LWDR retrieval accuracy, reducing the RMSE by approximately 23% compared to using the seven MODIS bands alone, fully illustrating the potential and importance of FIR bands under low WV conditions.

Under high WV conditions, the retrieval accuracy of all band types decreases. FIR bands face significant challenges due to their low transmittance in such atmospheres; the FIR spectrum becomes nearly opaque when WV exceeds 1 g cm^{-2} (Feldman et al. 2014). Similarly, TIR bands approach saturation under extremely high WV conditions, limiting their effectiveness. In contrast, joint bands, which combine MODIS and FIR, achieve significantly lower RMSE than the MODIS 7-band alone, highlighting the potential of joint bands in improving LWDR retrieval accuracy under such challenging scenarios.

These retrieval differences under varying WV conditions, as shown in Fig. 3, can be further explained by the behavior of FIR spectral transmittance under different atmospheric profiles. Comparing the transmission spectra for various climate zones in Fig. 4 reveals a vertical structure effect, most easily noticeable at a WV value of around 2 g cm^{-2}. If transmission

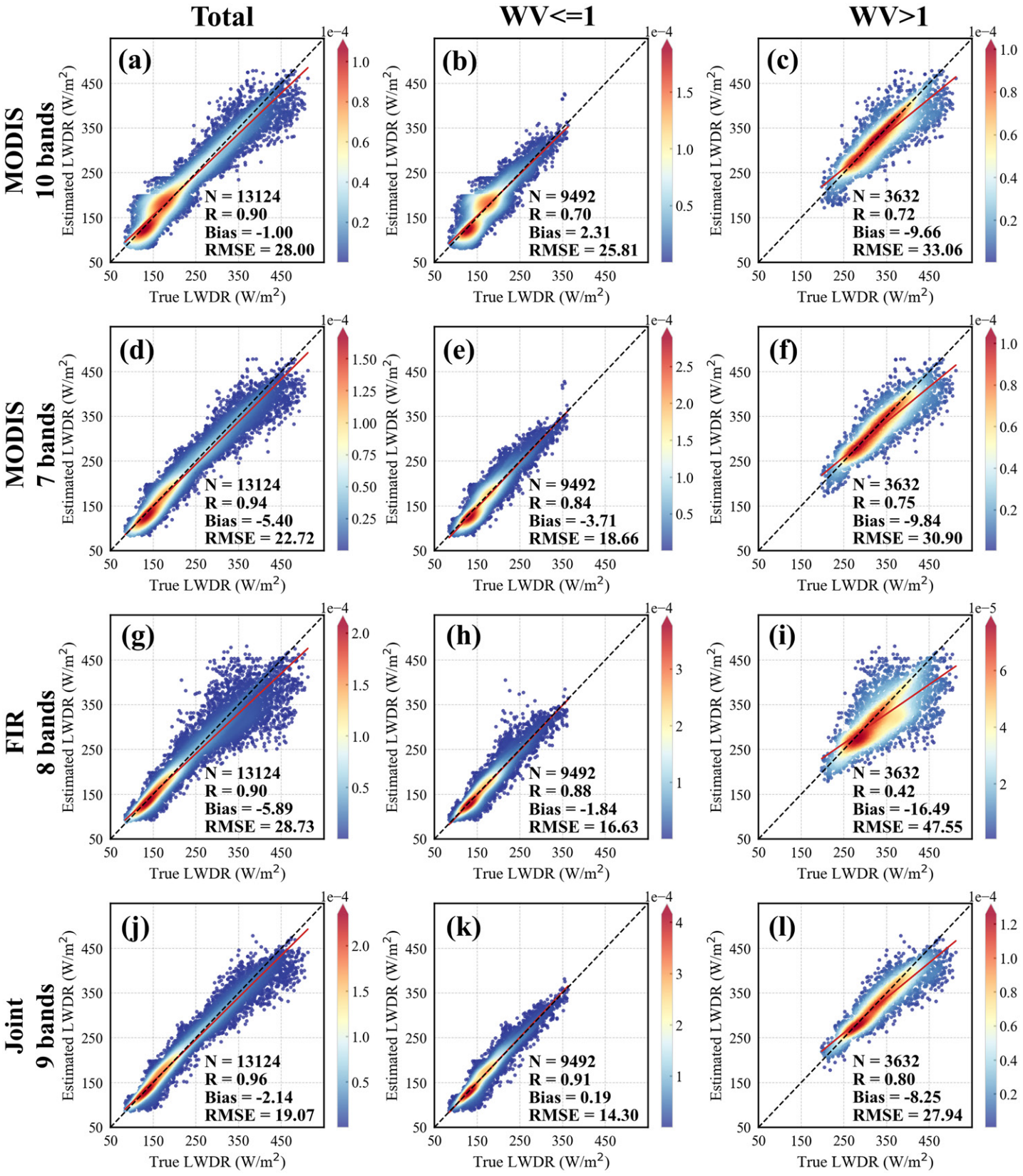

FIG. 3. Validation of LWDR retrieval accuracy using MODIS, FIR, and joint bands under overall, low- (WV < 1 g cm^{-2}), and high-WV (WV > 1 g cm^{-2}) conditions.

depended on the number of water molecules, it should rely only on WV, not climate. However, transmission for high-latitude atmospheres at the same water column is lower than for tropical atmospheres. The reason is the pressure dependence of absorption. To first order, absorption is proportional to pressure at most frequencies (Jeevanjee 2023), except at a few frequencies

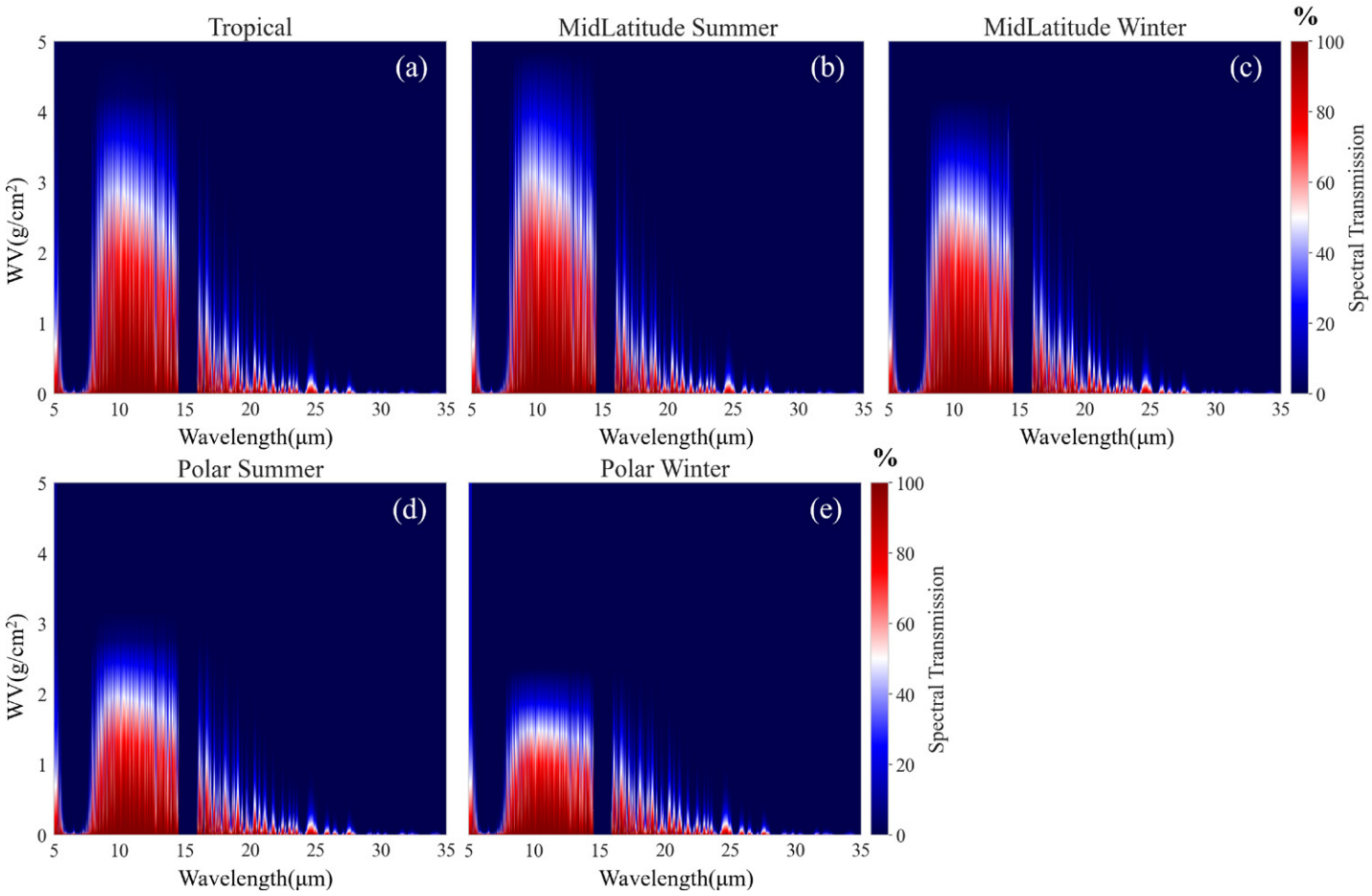

Fig. 4. Spectral transmission (surface to TOA) for various atmospheres and WV, calculated with MODTRAN6. Notably, in most atmospheric profiles, WV saturates at levels below 5 g cm^{-2}.

close to spectral lines. Since the temperature lapse rate is steeper at high latitudes, water vapor is confined to lower altitudes (higher pressure). Consequently, the absorption per water molecule is higher at high latitudes compared to the tropics.

These transmittance characteristics directly affect band performance. As WV increases, surface-to-atmosphere transmittance declines, while atmospheric emission becomes the dominant source of infrared radiation. When the WV content exceeds approximately 1 g·cm^{-2}, the FIR transmittance rapidly approaches zero (Fig. 4), causing the FIR channels to primarily sense radiation from the TOA rather than emissions from the surface or near-surface layers. This sharp reduction in transparency markedly decreases retrieval sensitivity and leads to a rapid increase in LWDR retrieval errors when relying solely on FIR bands (Fig. 3). Meanwhile, TIR channels also suffer from signal saturation under such humid conditions, further limiting their effectiveness. However, under low WV conditions, partially transparent dirty windows in the 17–26-μm range remain open, allowing retrieval of critical vertical profile information that complements the TIR signal and enhances LWDR accuracy. This effect is particularly pronounced in polar and high-altitude regions but also exists in tropical and midlatitude atmospheres during dry periods (Figs. 4a–c). Therefore, by jointly using FIR and TIR bands, it becomes possible to exploit the sensitivity of FIR microwindows in dry atmospheres and rely on the strong TIR signals to compensate for FIR attenuation in humid conditions, thereby achieving consistently superior LWDR retrieval accuracy across the full range of WV.

b. Antinoise performance analysis. Real remote sensing observations are subject to noise, which can impact the stability of LWDR retrievals. Based on the NEΔT values of the MODIS

and FIR bands (Table 1), random noise was introduced to all target bands. The noise was modeled as a normal distribution with a standard deviation defined as the NEΔT scaled by a noise amplification factor (factor = 0, 1, 2, 3) (Fig. 5). The MODIS TIR bands demonstrate high stability in accuracy, which explains their widespread use in LWDR estimation. However, the joint bands consistently achieve the highest accuracy among various combinations. Notably, under low WV conditions, the joint bands exhibit near-zero bias and are the only band combination with an R-value consistently above 0.9. Across different noise levels, the accuracy fluctuations of the joint bands are comparable to those of MODIS, demonstrating strong noise resistance. In contrast, FIR bands alone show the steepest decline in accuracy, particularly under high WV conditions. This suggests that FIR by itself may lack the stability required for reliable LWDR estimation. However, when FIR is combined with traditional TIR bands, the resulting joint bands outperform both stand-alone TIR and FIR configurations, providing superior accuracy and robustness under diverse conditions.

The retrieval accuracy of LWDR varies under different latitude zones and atmospheric conditions due to differences in temperature and water vapor content (Fig. 5). In tropical regions, high ST and WV obscure the transmissive windows of FIR bands, leading to poor retrieval performance when FIR bands are used alone. Conversely, polar areas, characterized by low temperatures and minimal WV, provide optimal conditions that significantly enhance the performance of the FIR band. When FIR bands are integrated with MODIS bands (joint 9 bands), retrieval accuracy improves substantially in tropical and midlatitude regions, with

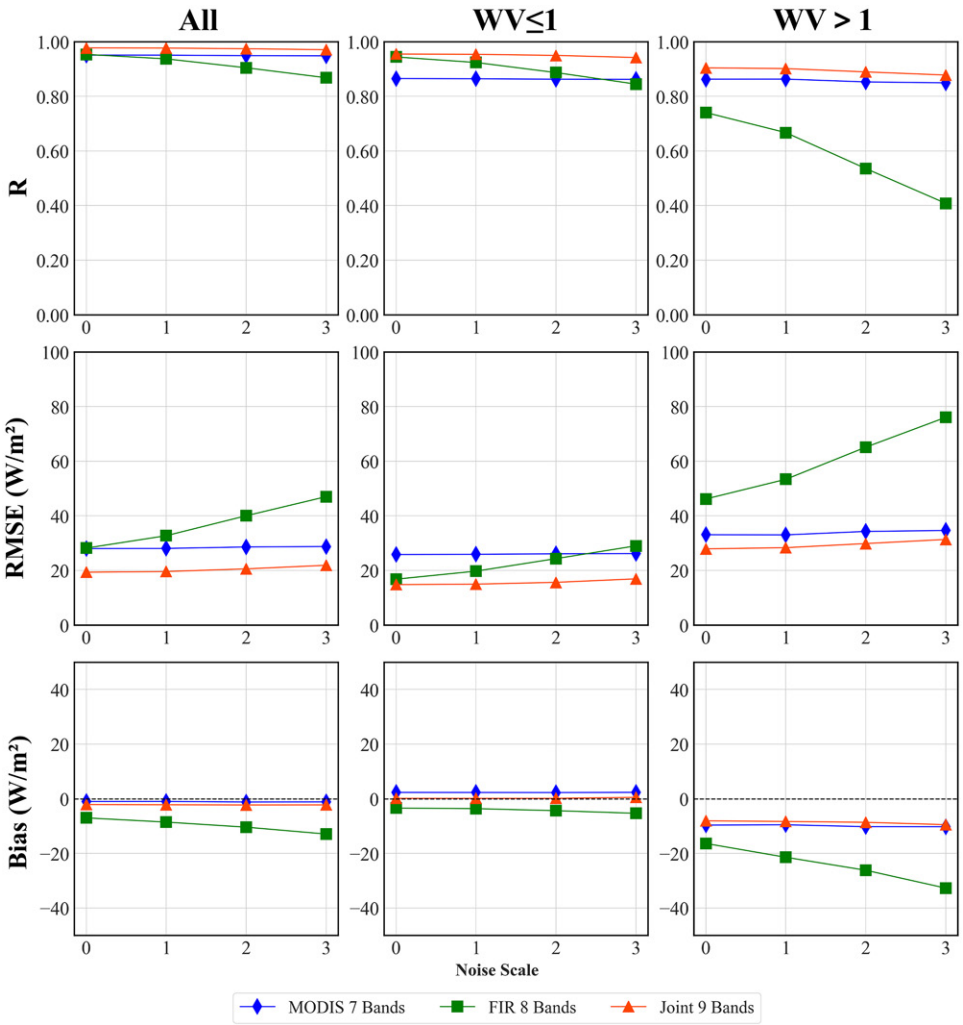

Fig. 5. Impact of noise on LWDR retrieval accuracy under different WV conditions (g cm^{-2}) for three band combinations.

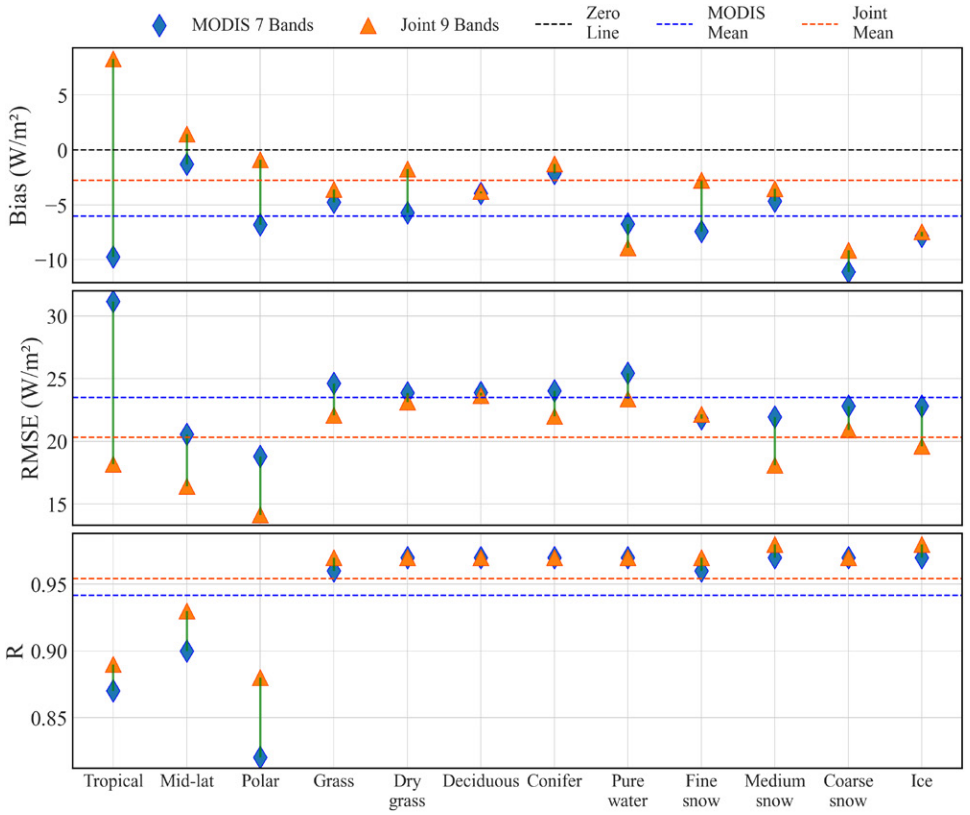

Fig. 6. LWDR retrieval accuracies using MODIS and joint bands under latitude zones and surface cover types after adding random noise (noise scale = 1).

RMSE reductions of 10% and 20%, respectively. In polar atmospheres, the joint 9 bands outperform FIR alone, achieving a 25% improvement in accuracy and demonstrating remarkable robustness. This improvement is attributed to the sensitivity of FIR bands to low WV conditions, which effectively complements the limitations of MODIS bands.

Different surface types, characterized by varying radiative properties and emissivity, also impact LWDR retrieval accuracy, though less strongly than the WV content. The FIR bands alone offer limited accuracy, primarily due to their low transmittance in all but low WV atmospheres and their greater sensitivity to atmospheric conditions than to surface characteristics. However, when integrated with MODIS bands, they provide a more comprehensive radiative dataset, ensuring accuracy and consistency across various surface types. Notably, on snow and ice surfaces, the joint 9 bands demonstrate superior performance compared to the MODIS 7 bands. Specifically, RMSE reductions of 13%, 17%, and 14% are observed for fine snow, medium snow, and ice surfaces, respectively. On fine snow, the bias is remarkably reduced by 63% (Fig. 6). This comprehensive analysis highlights the robustness and accuracy of incorporating FIR measurements into LWDR retrieval methodologies.

4. Advantages of including FIR bands in LWDR derivation

The estimation of all-sky longwave spectral flux has traditionally focused on the TIR spectral range. The estimation has primarily relied on a peak in the TIR, neglecting another significant peak in the FIR (Fig. 7).

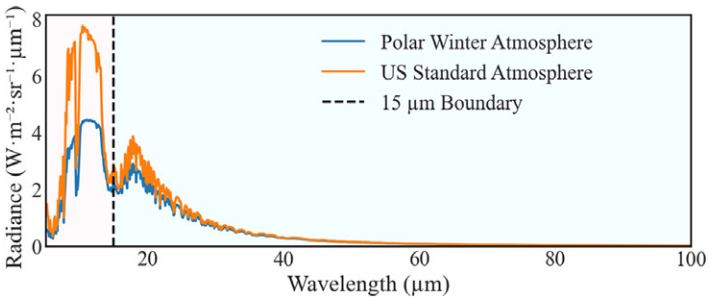

Fig. 7. Clear-sky radiance derived from the MODTRAN6 simulation of the *U.S. Standard Atmosphere* (orange) and the Polar Winter Atmosphere (blue).

Specifically, while polar observations exhibit distinct peaks in the TIR spectrum, a considerable portion of the spectral flux still occurs in the FIR range (L'Ecuyer et al. 2021). The integration of FIR and TIR bands completes the estimation across the entire spectral range, which explains the significant improvement in retrieval accuracy achieved with the joint 9 bands. This integration addresses previously overlooked spectral regions, offering a more comprehensive and accurate representation of Earth's radiation balance.

A BT sensitivity analysis was conducted to further evaluate the contributions of MODIS and FIR bands to clear-sky LWDR retrieval under polar conditions (Fig. 8). A detailed analysis of sensitivity to the key influencing factors, WV and ST, is provided in appendix C. Under cold and dry conditions, all MODIS TIR bands, except band 28, exhibited relatively weak variations in response to LWDR changes. MODIS band 28, a typical WV-sensitive band, demonstrated high sensitivity to LWDR, with consistent responses across surface types. MODIS band 33 displayed minimal changes within the low LWDR range (<150 W m^{-2}). In contrast, FIR bands

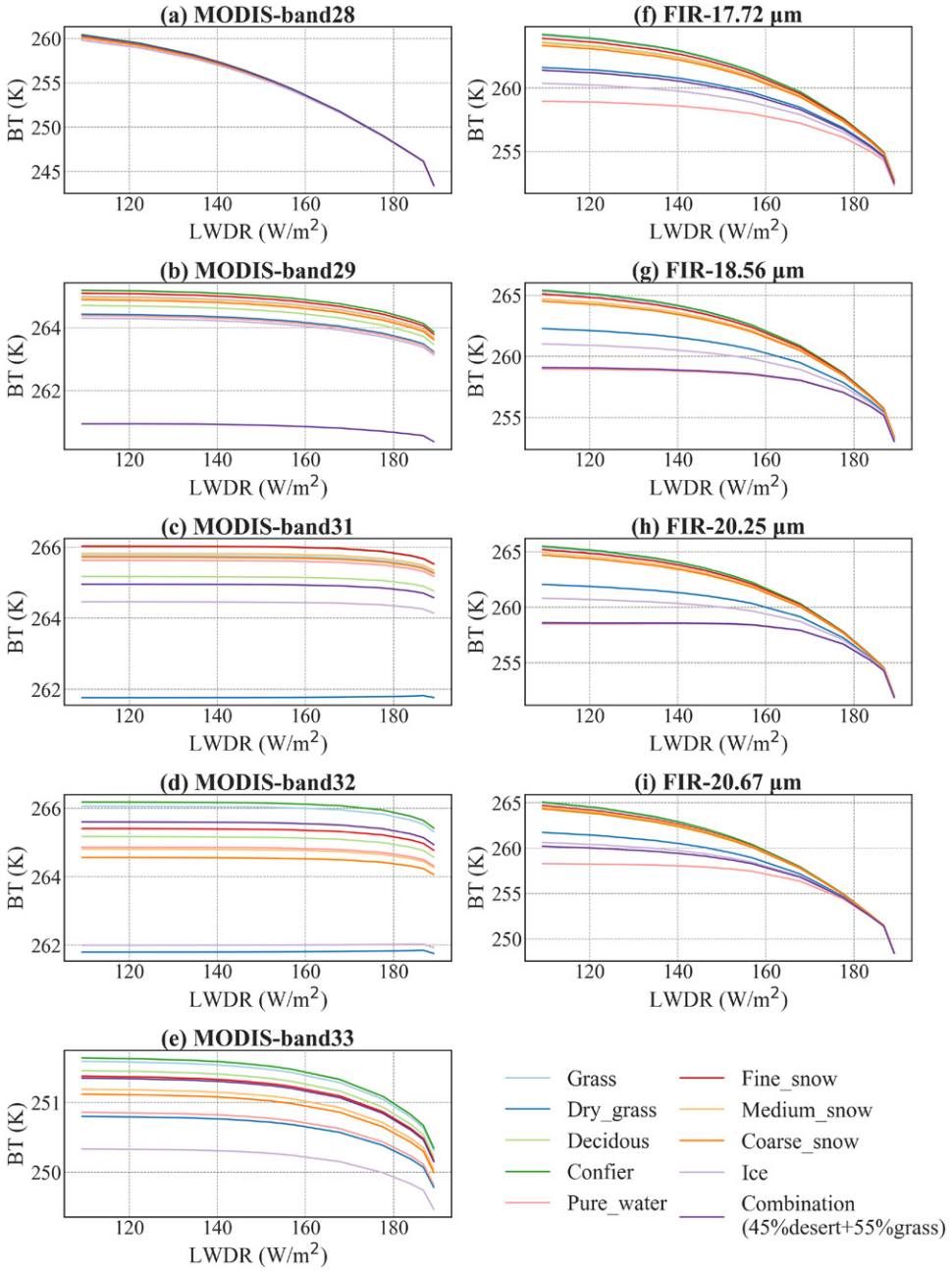

Fig. 8. Sensitivity analysis of MODIS and FIR bands to LWDR across different surface types under polar atmospheric conditions. The bands displayed are from the joint 9 bands.

were sensitive to LWDR and displayed varied response patterns across surface types. These characteristics further improved accuracy by compensating for the limitations of TIR bands under extreme conditions, ensuring stable LWDR retrieval across a range of conditions.

5. Exploring the potential of FIR for LWDR retrieval

This study integrates the FIR with traditional TIR bands, further confirming the value of FIR in LWDR estimation and focusing its potential application to the 15–20-μm range. FIR bands address the limitations of traditional TIR methods under very low WV conditions and show notable accuracy improvements, especially in cold, dry polar environments, effectively complementing TIR-based methods. Under high WV conditions, FIR bands have low transmittance, limiting their information content and applicability in warm, humid environments. In contrast, TIR bands accommodate higher WV levels to some extent but tend to saturate under extremely high WV conditions. Combining FIR and TIR bands provides a more comprehensive spectral range and ensures consistently high accuracy across various conditions, improving overall LWDR estimation accuracy by 16% and reducing RMSE by over 23% in polar regions.

This study overcomes the limitations of traditional TIR-based LWDR estimation methods and pioneers the exploration of FIR for clear-sky LWDR estimation. It provides theoretical support for current and upcoming FIR remote sensing missions, such as PREFIRE and FORUM. In particular, the forthcoming FORUM will deliver FWHM channels of 0.5 cm^{-1} (i.e., <0.14 μm), substantially finer than PREFIRE's. This enhanced spectral resolution is expected to increase the number of exploitable FIR "dirty window" channels, thereby further improving the accuracy of LWDR estimations. In this context, the present work offers insights into the further development of FIR-based LWDR retrieval.

Acknowledgments. This work was carried out under the co-funding of the National Natural Science Foundation of China projects (42371342), the Innovation Group Project of Southern Marine Science and Engineering Guangdong Laboratory (Zhuhai) (311022003), the China Scholarship Council program (Grant 202406380263), and the Zhuhai Basic and Applied Basic Research Project (ZH22017003200009PWC). The author extends sincere gratitude to the Meteorological Institute, Center for Earth System Research and Sustainability (CEN), University of Hamburg for their invaluable support and resources provided during the author's visit.

Data availability statement. The simulation datasets generated in this study are not proactively archived in public repositories due to their substantial volume and relevance to ongoing research. However, they are accessible upon request by contacting the corresponding author at wangtx23@mail.sysu.edu.cn. Reproducibility details are fully documented in the main text and the appendix of the article.

APPENDIX A

Conservative Noise Sensitivity Analysis

Based on PREFIRE specifications, an NEΔT of less than 1.1 K is specified for the 12–25-μm range, encompassing the channels selected for this study. The mission also specifies an NEΔT of less than 1.5 K (at 300 K) for all FIR channels. To evaluate the impact of noise on retrieval performance, a NEΔT of 1.5 K was applied to the simulated FIR bands as a conservative estimate (Fig. A1). For the TIR bands, channel-specific NEΔT values corresponding to the relevant MODIS bands were used, consistent with the typical performance of this instrument.

The results indicate that FIR measurement quality significantly affects LWDR retrieval accuracy. While including FIR bands generally improves performance over using TIR alone,

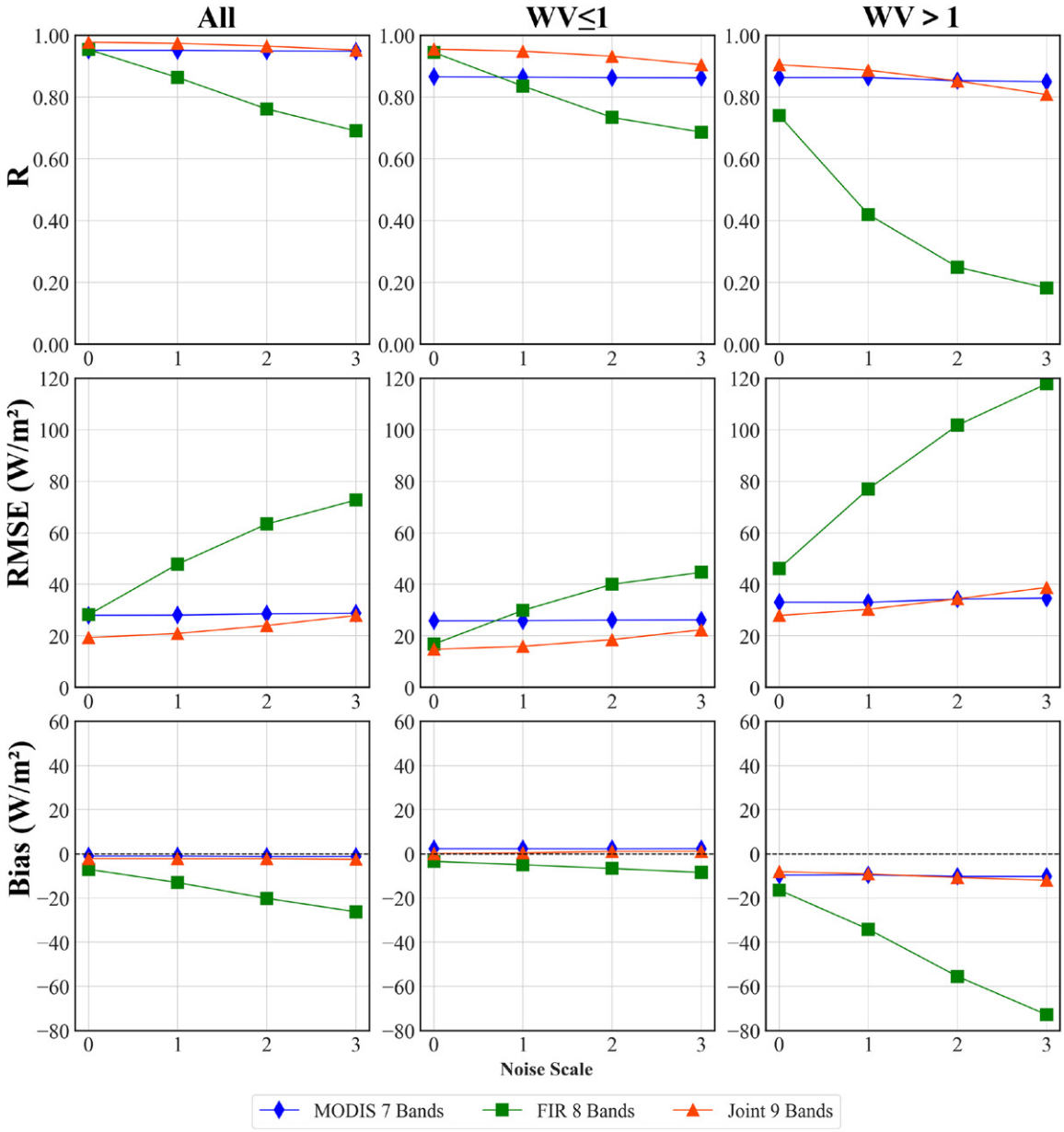

Fig. A1. Impact of noise (NEΔT = 1.5 K for FIR) on LWDR retrieval accuracy under different WV conditions (g cm^{-2}) for three band combinations.

the retrieval accuracy decreases to be comparable to or even slightly lower than that of TIR when FIR noise is substantially increased (i.e., NEΔT = 1.5 K with an amplification factor of 3). This highlights the critical need for high-quality FIR measurements.

APPENDIX B

Algorithm and Validation Strategy

In this study, a lookup table (LUT) method is used to calculate clear-sky LWDR. The LUT is subdivided into sub-tables according to the viewing zenith angle and altitude. Within each sub-table, the 15 records closest to the target pixel, based on the BT of each channel, are selected, and the mean value is taken after outlier filtering. The similarity between the records in the LUT and the target pixel is calculated using the Euclidean distance. The simulation conditions for constructing the LUT with MODTRAN 6 are shown in Table B1.

A simulated validation dataset is employed to verify and confirm the theoretical accuracy of incorporating FIR for clear-sky LWDR retrieval. The randomly generated simulation

Table B1. Settings of MODTRAN parameters when generating the LUT dataset.

Parameters	Setting
Viewing zenith angle	0, 10, 20, 30, 40, 50, 60, 65, 70
Atmosphere model	89 TIGR profiles
Surface albedo	16 land-cover spectra
Land surface temperature (K)	Base temperature of the atmospheric profile ±15 K with an increment of 3 K
Aerosol	Default rural, VIS = 23 km
WV (g cm^{-2})	(0.004, 6.8) with an increment of 0.15

Table B2. Settings of MODTRAN parameters when generating the simulated validation dataset. The *x* means a random value, and T_0 is the base temperature of the atmospheric profile.

Parameters	Setting
Viewing zenith angle (°)	$x \in [0, 65]$
Atmosphere model	946 TIGR clear-sky atmospheric profiles
Surface albedo	26 land-cover spectra
Land surface temperature (K)	$x \in [T_0 - 6, T_0 + 12]$
Aerosol type	Rural, maritime, urban
VIS (km)	$x \in [1, 100]$
WV (g cm^{-2})	$x \in [0.004, 6.8]$
Surface altitude (km)	$x \in [0, 5.9]$

conditions are based on Table B2. Through random simulation, 15 000 simulation records were generated. After excluding unreasonable results, such as WV oversaturation under clear-sky conditions, a total of over 13 000 valid sample points were obtained.

APPENDIX C
Sensitivity Analysis

As shown in Fig. C1, MODIS bands 31 and 32 are commonly used to calculate BT differences as indicators of WV variation. However, their performance is limited under cold and dry conditions (Li et al. 2024), which directly affects the accuracy of the atmospheric WV profile required for LWDR retrieval. Band 28 exhibits high sensitivity to WV, but with consistent responses across different surface types. MODIS window bands (29, 31, and 32) show strong sensitivity to ST, suggesting they primarily capture surface signals rather than atmospheric temperature signals, which may not be optimal for LWDR retrieval.

Since clear-sky LWDR is mainly determined by atmospheric temperature and WV profiles, the relatively weak BT response of FIR bands to ST, combined with their substantially higher sensitivity to WV compared to MODIS TIR bands, indicates that FIR bands are more focused on atmospheric properties. This makes them more suitable for LWDR retrieval than certain MODIS bands.

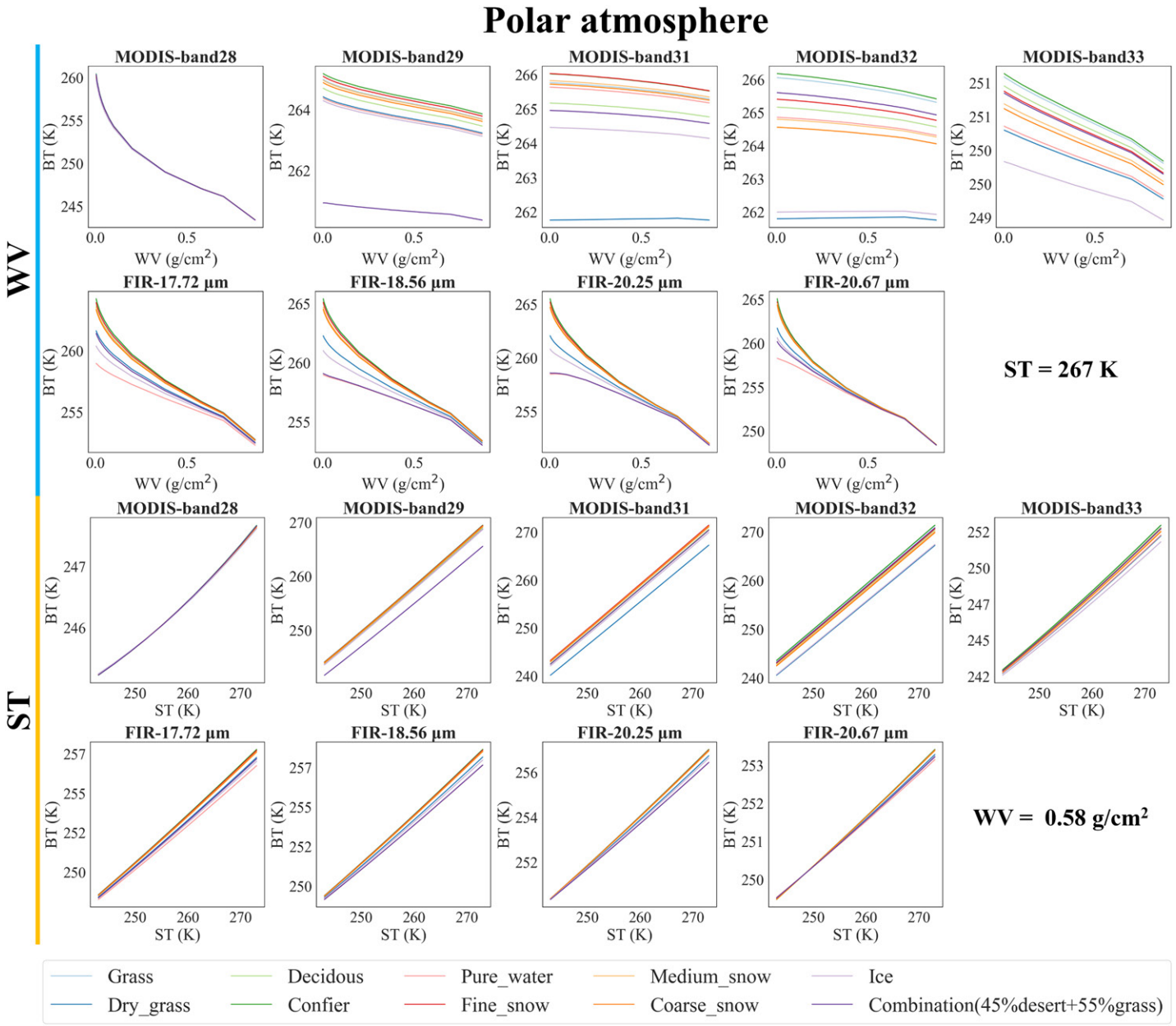

Fig. C1. Sensitivity analysis of MODIS and FIR bands to WV and ST across different surface types under polar atmospheric conditions. The bands displayed are from the joint 9 bands.

References

Agocs, T., and Coauthors, 2022: Far-infrared outgoing radiation understanding and monitoring (Forum)—System overview and key technology developments of ESA's 9th Earth explorer. *IEEE Int. Geoscience and Remote Sensing Symp. (IGARSS)*, Kuala Lumpur, Malaysia, Institute of Electrical and Electronics Engineers, 7186–7189, https://doi.org/10.1109/IGARSS46834.2022.9883892.

Belotti, C., and Coauthors, 2023: The Far-Infrared Radiation Mobile Observation System (FIRMOS) for spectral characterization of the atmospheric emission. *Atmos. Meas. Tech.*, **16**, 2511–2529, https://doi.org/10.5194/amt-16-2511-2023.

Berk, A., P. Conforti, and F. Hawes, 2015: An accelerated line-by-line option for MODTRAN (R) combining on-the-fly generation of line center absorption within 0.1 cm-1 bins and pre-computed line tails. *Proc. SPIE*, **9472**, 947217, https://doi.org/10.1117/12.2177444.

Bertossa, C., T. L'Ecuyer, A. Merrelli, X. L. Huang, and X. H. Chen, 2023: A neural network–based cloud mask for PREFIRE and evaluation with simulated observations. *J. Atmos. Oceanic Technol.*, **40**, 377–396, https://doi.org/10.1175/JTECH-D-22-0023.1.

Bianchini, G., F. Castagnoli, G. Di Natale, and L. Palchetti, 2019: A Fourier transform spectroradiometer for ground-based remote sensing of the atmospheric downwelling long-wave radiance. *Atmos. Meas. Tech.*, **12**, 619–635, https://doi.org/10.5194/amt-12-619-2019.

Cao, Y. F., M. Y. Li, and Y. Z. Zhang, 2022: Estimating the clear-sky longwave downward radiation in the arctic from FengYun-3D MERSI-2 data. *Remote Sens.*, **14**, 606, https://doi.org/10.3390/rs14030606.

Chang, K.-W., T. S. L'Ecuyer, B. H. Kahn, and V. Natraj, 2017: Information content of visible and midinfrared radiances for retrieving tropical ice cloud properties. *J. Geophys. Res. Atmos.*, **122**, 4944–4966, https://doi.org/10.1002/2016JD026357.

Chedin, A., N. A. Scott, C. Wahiche, and P. Moulinier, 1985: The improved initialization inversion method: A high resolution physical method for temperature retrievals from satellites of the TIROS-N series. *J. Climate Appl. Meteor.*, **24**, 128–143, https://doi.org/10.1175/1520-0450(1985)024<0128:TIIIMA>2.0.CO;2.

Chen, B. Y., and Z. Z. Liu, 2016: Global water vapor variability and trend from the latest 36 year (1979 to 2014) data of ECMWF and NCEP reanalyses, radiosonde, GPS, and microwave satellite. *J. Geophys. Res. Atmos.*, **121**, 11 442–11 462, https://doi.org/10.1002/2016JD024917.

Chen, X., X. Huang, and M. G. Flanner, 2014: Sensitivity of modeled far-IR radiation budgets in polar continents to treatments of snow surface and ice cloud radiative properties. *Geophys. Res. Lett.*, **41**, 6530–6537, https://doi.org/10.1002/2014GL061216.

Cheng, J., S. L. Liang, W. H. Wang, and Y. M. Guo, 2017: An efficient hybrid method for estimating clear-sky surface downward longwave radiation from MODIS data. *J. Geophys. Res. Atmos.*, **122**, 2616–2630, https://doi.org/10.1002/2016JD026250.

Chevallier, F., F. Chéruy, N. A. Scott, and A. Chédin, 1998: A neural network approach for a fast and accurate computation of a longwave radiative budget. *J. Appl. Meteor.*, **37**, 1385–1397, https://doi.org/10.1175/1520-0450(1998)037<1385:ANNAFA>2.0.CO;2.

Conrath, B. J., R. A. Hanel, V. G. Kunde, and C. Prabhakara, 1970: The infrared interferometer experiment on Nimbus 3. *J. Geophys. Res.*, **75**, 5831–5857, https://doi.org/10.1029/JC075i030p05831.

Cox, C. V., J. E. Harries, J. P. Taylor, P. D. Green, A. J. Baran, J. C. Pickering, A. E. Last, and J. E. Murray, 2010: Measurement and simulation of mid- and far-infrared spectra in the presence of cirrus. *Quart. J. Roy. Meteor. Soc.*, **136**, 718–739, https://doi.org/10.1002/qj.596.

Di Natale, G., G. Bianchini, M. Del Guasta, M. Ridolfi, T. Maestri, W. Cossich, D. Magurno, and L. Palchetti, 2020: Characterization of the far infrared properties and radiative forcing of Antarctic ice and water clouds exploiting the Spectrometer-LiDAR synergy. *Remote Sens.*, **12**, 3574, https://doi.org/10.3390/rs12213574.

Feldman, D. R., W. D. Collins, R. Pincus, X. L. Huang, and X. H. Chen, 2014: Far-infrared surface emissivity and climate. *Proc. Natl. Acad. Sci. USA*, **111**, 16 297–16 302, https://doi.org/10.1073/pnas.1413640111.

Hanel, R. A., B. Schlachman, D. Rogers, and D. Vanous, 1971: Nimbus 4 Michelson interferometer. *Appl. Opt.*, **10**, 1376–1382, https://doi.org/10.1364/AO.10.001376.

Harries, J., and Coauthors, 2008: The far-infrared Earth. *Rev. Geophys.*, **46**, RG4004, https://doi.org/10.1029/2007RG000233.

Huang, X., J. N. S. Cole, F. He, G. L. Potter, L. Oreopoulos, D. Lee, M. Suarez, and N. G. Loeb, 2013: Longwave band-by-band cloud radiative effect and its application in GCM evaluation. *J Climate*, **26**, 450–467, https://doi.org/10.1175/JCLI-D-12-00112.1.

——, X. Chen, D. K. Zhou, and X. Liu, 2016: An observationally based global band-by-band surface emissivity dataset for climate and weather simulations. *J. Atmos. Sci.*, **73**, 3541–3555, https://doi.org/10.1175/JAS-D-15-0355.1.

——, ——, B. J. Drouin, T. I. Michaels, and E. H. Wagner, 2025: Polar Radiant Energy in the Far-Infrared Experiment (PREFIRE) Algorithm Theoretical Basis Document (ATBD) for the 2B-FLX data product. PREFIRE ATBDs, 27 pp., https://prefire.ssec.wisc.edu/Documents/ATBD/PREFIRE_2B-FLX_ATBD-20250430.pdf.

Huang, Y., V. Ramaswamy, X. L. Huang, Q. Fu, and C. Bardeen, 2007: A strict test in climate modeling with spectrally resolved radiances: GCM simulation versus AIRS observations. *Geophys. Res. Lett.*, **34**, L24707, https://doi.org/10.1029/2007GL031409.

Inamdar, A. K., and V. Ramanathan, 1997: On monitoring the atmospheric greenhouse effect from space. *Tellus*, **49B**, 216, https://doi.org/10.3402/tellusb.v49i2.15963.

Jeevanjee, N., 2023: Climate sensitivity from radiative-convective equilibrium: A chalkboard approach. *Amer. J. Phys.*, **91**, 731–745, https://doi.org/10.1119/5.0135727.

Jiao, Z. H., and X. H. Mu, 2022: Global validation of clear-sky models for retrieving land-surface downward longwave radiation from MODIS data. *Remote Sens. Environ.*, **271**, 112903, https://doi.org/10.1016/j.rse.2022.112903.

Kapsch, M. L., R. G. Graversen, and M. Tjernström, 2013: Springtime atmospheric energy transport and the control of Arctic summer sea-ice extent. *Nat. Climate Change*, **3**, 744–748, https://doi.org/10.1038/nclimate1884.

Kratz, D. P., S. K. Gupta, A. C. Wilber, and V. E. Sothcott, 2020: Validation of the CERES edition-4A surface-only flux algorithms. *J. Appl. Meteor. Climatol.*, **59**, 281–295, https://doi.org/10.1175/JAMC-D-19-0068.1.

L'Ecuyer, T. S., and Coauthors, 2021: The polar radiant energy in the far infrared experiment: A new perspective on polar longwave energy exchanges. *Bull. Amer. Meteor. Soc.*, **102**, E1431–E1449, https://doi.org/10.1175/BAMS-D-20-0155.1.

Lee, S., T. Gong, S. B. Feldstein, J. A. Screen, and I. Simmonds, 2017: Revisiting the cause of the 1989–2009 Arctic surface warming using the surface energy budget: Downward infrared radiation dominates the surface fluxes. *Geophys. Res. Lett.*, **44**, 10 654–10 661, https://doi.org/10.1002/2017GL075375.

Li, D., and Coauthors, 2024: Multi-Dimensional matrix MAPping (MDMAP): A new algorithm framework to derive top-of-atmosphere outgoing longwave radiation from space. *Remote Sens. Environ.*, **304**, 114031, https://doi.org/10.1016/j.rse.2024.114031.

Liang, S. L., D. D. Wang, T. He, and Y. Y. Yu, 2019: Remote sensing of Earth's energy budget: Synthesis and review. *Int. J. Digital Earth*, **12**, 737–780, https://doi.org/10.1080/17538947.2019.1597189.

Martinazzo, M., and T. Maestri, 2023: The MAMA algorithm for fast computations of upwelling far- and mid-infrared radiances in the presence of clouds. *Remote Sens.*, **15**, 4454, https://doi.org/10.3390/rs15184454.

Marty, C., and Coauthors, 2003: Downward longwave irradiance uncertainty under arctic atmospheres: Measurements and modeling. *J. Geophys. Res.*, **108**, 4358, https://doi.org/10.1029/2002JD002937.

Miller, N. B., A. Merrelli, T. S. L'ecuyer, and B. J. Drouin, 2023: Simulated clear-sky water vapor and temperature retrievals from PREFIRE measurements. *J. Atmos. Oceanic Technol.*, **40**, 645–659, https://doi.org/10.1175/JTECH-D-22-0128.1.

Mlynczak, M. G., R. P. Cageao, J. C. Mast, D. P. Kratz, H. Latvakoski, and D. G. Johnson, 2016: Observations of downwelling far-infrared emission at Table Mountain California made by the FIRST instrument. *J. Quant. Spectrosc. Radiat. Transfer*, **170**, 90–105, https://doi.org/10.1016/j.jqsrt.2015.10.017.

Palchetti, L., and Coauthors, 2020: FORUM: Unique Far-Infrared satellite observations to better understand how Earth radiates energy to space. *Bull. Amer. Meteor. Soc.*, **101**, E2030–E2046, https://doi.org/10.1175/BAMS-D-19-0322.1.

——, and Coauthors, 2021: Observations of the downwelling far-infrared atmospheric emission at the Zugspitze observatory. *Earth Syst. Sci. Data*, **13**, 4303–4312, https://doi.org/10.5194/essd-13-4303-2021.

Peterson, C. A., X. H. Chen, Q. Yue, and X. L. Huang, 2019: The spectral dimension of Arctic outgoing longwave radiation and greenhouse efficiency trends from 2003 to 2016. *J. Geophys. Res. Atmos.*, **124**, 8467–8480, https://doi.org/10.1029/2019JD030428.

——, X. L. Huang, X. H. Chen, and P. Yang, 2022: Synergistic use of far- and mid-infrared spectral radiances for satellite-based detection of polar ice clouds over ocean. *J. Geophys. Res. Atmos.*, **127**, e2021JD035733, https://doi.org/10.1029/2021JD035733.

Rathke, C., J. Fischer, S. Neshyba, and M. Shupe, 2002: Improving IR cloud phase determination with 20 microns spectral observations. *Geophys. Res. Lett.*, **29**, 1209, https://doi.org/10.1029/2001GL014594.

Rodgers, C. D., 2000: *Inverse Methods for Atmospheric Sounding: Theory and Practice.* World Scientific, 256 pp.

Ruckstuhl, C., R. Philipona, J. Morland, and A. Ohmura, 2007: Observed relationship between surface specific humidity, integrated water vapor, and longwave downward radiation at different altitudes. *J. Geophys. Res.*, **112**, D03302, https://doi.org/10.1029/2006JD007850.

Schmetz, J., 1989: Towards a surface radiation climatology: Retrieval of downward irradiances from satellites. *Atmos. Res.*, **23**, 287–321, https://doi.org/10.1016/0169-8095(89)90023-9.

Sobrino, J. A., and J. C. Jiménez-Muñoz, 2014: Minimum configuration of thermal infrared bands for land surface temperature and emissivity estimation in the context of potential future missions. *Remote Sens. Environ.*, **148**, 158–167, https://doi.org/10.1016/j.rse.2014.03.027.

Stephens, G. L., M. Wild, P. W. Stackhouse, T. L'Ecuyer, S. Kato, and D. S. Henderson, 2012: The global character of the flux of downward longwave radiation. *J. Climate*, **25**, 2329–2340, https://doi.org/10.1175/JCLI-D-11-00262.1.

Trenberth, K. E., and J. T. Fasullo, 2012: Tracking Earth's energy: From El Niño to global warming. *Surv. Geophys.*, **33**, 413–426, https://doi.org/10.1007/s10712-011-9150-2.

——, ——, and J. Kiehl, 2009: Earth's global energy budget. *Bull. Amer. Meteor. Soc.*, **90**, 311–324, https://doi.org/10.1175/2008BAMS2634.1.

Turner, D. D., P. J. Gero, and D. C. Tobin, 2012a: The far-infrared: Focusing on a relatively underexplored portion of the electromagnetic spectrum. *Bull. Amer. Meteor. Soc.*, **93**, ES103–ES104, https://doi.org/10.1175/BAMS-D-12-00007.1.

——, A. Merrelli, D. Vimont, and E. J. Mlawer, 2012b: Impact of modifying the longwave water vapor continuum absorption model on Community Earth System Model simulations. *J. Geophys. Res.*, **117**, D04106, https://doi.org/10.1029/2011JD016440.

Wang, K. C., and R. E. Dickinson, 2013: Global atmospheric downward longwave radiation at the surface from ground-based observations, satellite retrievals, and reanalyses. *Rev. Geophys.*, **51**, 150–185, https://doi.org/10.1002/rog.20009.

Wild, M., D. Folini, C. Schär, N. Loeb, E. G. Dutton, and G. König-Langlo, 2013: The global energy balance from a surface perspective. *Climate Dyn.*, **40**, 3107–3134, https://doi.org/10.1007/s00382-012-1569-8.

Xie, Y., X. Huang, X. Chen, T. S. L'Ecuyer, B. J. Drouin, and J. Wang, 2022: Retrieval of surface spectral emissivity in polar regions based on the optimal estimation method. *J. Geophys. Res. Atmos.*, **127**, e2021JD035677, https://doi.org/10.1029/2021JD035677.

——, ——, ——, ——, and ——, 2023: Joint use of far-infrared and mid-infrared observation for sounding retrievals: Learning from the past for upcoming far-infrared missions. *Earth Space Sci.*, **10**, e2022EA002684, https://doi.org/10.1029/2022EA002684.

Yan, H. R., J. P. Huang, P. Minnis, T. H. Wang, and J. R. Bi, 2011: Comparison of CERES surface radiation fluxes with surface observations over Loess Plateau. *Remote Sens. Environ.*, **115**, 1489–1500, https://doi.org/10.1016/j.rse.2011.02.008.

Yang, K., T. Koike, P. Stackhouse, C. Mikovitz, and S. J. Cox, 2006: An assessment of satellite surface radiation products for highlands with Tibet instrumental data. *Geophys. Res. Lett.*, **33**, L22403, https://doi.org/10.1029/2006GL027640.

Zheng, X. P., Z. L. Li, F. Nerry, and X. Zhang, 2019: A new thermal infrared channel configuration for accurate land surface temperature retrieval from satellite data. *Remote Sens. Environ.*, **231**, 111216, https://doi.org/10.1016/j.rse.2019.111216.